

# Optomechanical Anti-Lasing with Infinite Group Delay at a Phase Singularity

Yulong Liu<sup>1,2</sup>, Qichun Liu<sup>1</sup>, Shuaipeng Wang<sup>3</sup>, Zhen Chen<sup>1</sup>, Mika A. Sillanpää<sup>2,\*</sup> and Tiefu Li<sup>4,1,†</sup>

<sup>1</sup>*Beijing Academy of Quantum Information Sciences, Beijing 100193, China*

<sup>2</sup>*Department of Applied Physics, Aalto University, P.O. Box 15100, FI-00076 Aalto, Finland*

<sup>3</sup>*Quantum Physics and Quantum Information Division, Beijing Computational Science Research Center, Beijing 100193, China*

<sup>4</sup>*School of Integrated Circuits and Frontier Science Center for Quantum Information, Tsinghua University, Beijing 100084, China*



(Received 31 August 2021; revised 15 November 2021; accepted 10 December 2021; published 29 December 2021)

Singularities which symbolize abrupt changes and exhibit extraordinary behavior are of a broad interest. We experimentally study optomechanically induced singularities in a compound system consisting of a three-dimensional aluminum superconducting cavity and a metalized high-coherence silicon nitride membrane resonator. Mechanically induced coherent perfect absorption and anti-lasing occur simultaneously under a critical optomechanical coupling strength. Meanwhile, the phase around the cavity resonance undergoes an abrupt  $\pi$ -phase transition, which further flips the phase slope in the frequency dependence. The observed infinite discontinuity in the phase slope defines a singularity, at which the group velocity is dramatically changed. Around the singularity, an abrupt transition from an infinite group advance to delay is demonstrated by measuring a Gaussian-shaped waveform propagating. Our experiment may broaden the scope of realizing extremely long group delays by taking advantage of singularities.

DOI: [10.1103/PhysRevLett.127.273603](https://doi.org/10.1103/PhysRevLett.127.273603)

Electromagnetically induced transparency (EIT), where a transmission window is induced within an absorption resonance, arises from the destructive quantum interference of different excitation pathways [1–3]. As a counterpart of EIT, electromagnetically induced absorption (EIA) accompanied by a substantial enhancement of the absorption rate of a probe field [4–9] also has received considerable attention due to its versatile applications such as enhancing photodetection [10–12], giant Faraday rotation [13], and high-precise quantum sensing [14–16]. In contrast to EIT introduced by destructive quantum interference, the observed EIA arises due to the constructive interference between different excitation pathways [17–20]. In particular, the incident electromagnetic field can be perfectly absorbed by precisely controlling the constructive interference [21–25]. Coherent perfect absorption (CPA) is achieved when the dip of the EIA spectrum approaches zero [26–29]. Intriguing applications through the CPA include synthetic reflectionless media [30–32], time-reversed lasers [33–36], and random anti-lasing [37].

The above intriguing applications are closely related to the amplitude responses of light transmission. Meanwhile, the phase also exhibits interesting properties, e.g., EIT and EIA with unique behaviors of dispersion [38–43] could lead to group delay (slow light) or advance (fast light), respectively. Classical analogs for EIT and EIA have been simultaneously demonstrated in a variety platforms such as plasmonics [44], metamaterials [45], and optical resonators [46]. Similar to EIT and EIA realized through mechanical effects of light [47–49], optomechanically induced transparency (OMIT) and absorption (OMIA)

are also caused by destructive and constructive pathway interferences [50–55], respectively. In the microwave domain, OMIT [56–60] and OMIA [61–64] have been demonstrated in electromechanical devices where a superconducting microwave resonator couples to a mechanical resonator realized as a capacitor [65–67]. Integrating electromechanics with solid-state qubits, e.g., superconducting qubits [68–72], leads to a promising hybrid architecture for a quantum repeater [73]. The parametric optomechanical coupling has a great tunability. Change of probe light transmission from absorption to transparency or amplification has been experimentally observed by tuning the power of a blue-detuned sideband pump [61]. The probe light could be completely absorbed and fast-slow light conversion occurs at a critical pump power [74]. The amplitude and phase of the cavity output photons are both measurable. Therefore, optomechanical systems provide an ideal experimental platform to study how CPA affects the phase evolution, and allow us to study fast-slow light transition, and then explore an ultralong group delay around this phase singularity.

*The device.*—As shown in Fig. 1(a), the cavity electromechanical device consists of a three-dimensional (3D) superconducting aluminum (Al) cavity and a mechanically compliant capacitor. The external coupling strength is adjusted by the protrusion length of the Sub-Miniature A (SMA) connector's pin inside the cavity. The dark-red interference fringes within the narrow capacitor gap indicate that the distance is at a few hundred nanometers level. The schematic in Fig. 1(b) shows how the metalized silicon nitride (SiN) membrane is flip-chip mounted over the

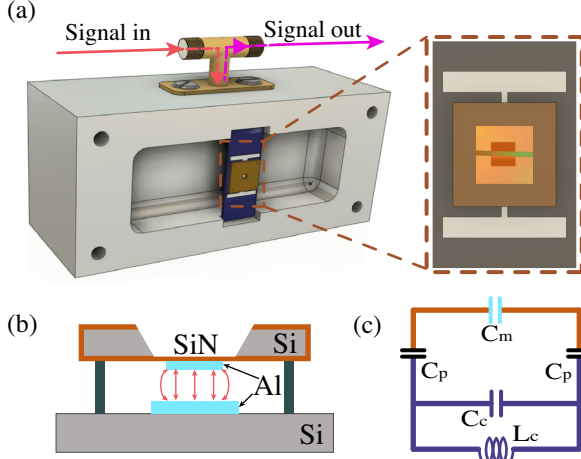


FIG. 1. (a) The 3D microwave cavity and a mechanically compliant capacitor. Microwave signals couple in and out of the cavity through a common connector. (b) Schematic showing the placement of the metalized membrane over the antenna pads. (c) Lumped-element model consists of cavity capacitance  $C_c$ , inductance  $L_c$ , antenna-cavity coupling capacitance  $C_p$ , and the mechanical capacitance  $C_m$ .

bottom antenna pads. Detailed fabrication and packaging processes are presented in the Supplemental Material [75]. The H-shaped antenna is used to enhance the electro-mechanical coupling. The choice of a high-stress SiN membrane as the mechanical resonator is motivated by its high- $Q$  performance at millikelvin temperatures [76–81].

The equivalent lumped-element model of the cavity and membrane capacitor is shown in Fig. 1(c). The vibration of the SiN membrane changes the capacitance of the circuit resonator and causes a change in its resonant frequency. Therefore, a dispersive optomechanical coupling is formed. A coherent pump tone with frequency  $\Omega_c$  and amplitude  $\xi$  is used to enhance the optomechanical coupling [65]. In this experiment, the pump frequency is red-detuned from the cavity resonant frequency ( $\omega_c$ ) by the mechanical frequency ( $\omega_m$ ), i.e.,  $\Omega_c = \omega_c - \omega_m$ . A weak coherent probe field with frequency  $\Omega_p$  and amplitude  $\varepsilon$  is used to measure the transmission response. Working in the rotating frame at the pump-tone frequency, the linearized Hamiltonian is given as

$$H/\hbar = \Delta(a^\dagger a + b^\dagger b) + G(a^\dagger b + b^\dagger a) + i\sqrt{\eta\kappa}(\varepsilon a^\dagger - \varepsilon^* a). \quad (1)$$

The cavity mode is described by the bosonic operators  $a$  ( $a^\dagger$ ) and the mechanical mode is described by  $b$  ( $b^\dagger$ ), respectively. The detuning is defined as  $\Delta = \omega_c - \Omega_p$ . Here,  $G = g\sqrt{\bar{n}_c}$  is the linearized and field-enhanced coupling strength. The quantity  $g$  is the single-photon optomechanical coupling rate and  $\bar{n}_c$  is the average number of photons in the cavity. Thus, the cavity-mechanics

coupling rate  $G$  can be continuously adjusted by controlling the power of the coherent pump tone. Without loss of generality,  $G$  is assumed to be a real number. The coupling to the SMA connector results in an external decay rate of  $\kappa_e$ . The cavity mode can be characterized by a total loss  $\kappa$  and the external coupling parameter  $\eta = \kappa_e/\kappa$ . By considering the input-output relations, the transmission coefficient is given as

$$t = 1 - \frac{\eta\kappa(i\Delta + \gamma_m/2)}{(i\Delta + \gamma_m/2)(i\Delta + \kappa/2) + G^2}, \quad (2)$$

where  $\gamma_m$  represents the decay rate of the mechanical mode. The amplitude and phase responses are given as  $T = |t|^2$ , and  $\varphi = \arg(t)$ , respectively. The transmission at cavity resonance with zero detuning (setting  $\Delta$  to be zero) becomes

$$t_z = \frac{G^2 - (\eta - 1/2)\kappa\gamma_m/2}{G^2 + \kappa\gamma_m/4}. \quad (3)$$

At zero detuning,  $t_z$  is always a real number. Setting  $t_z$  to be zero yields a critical coupling  $G_c = \sqrt{(\eta - 1/2)\kappa\gamma_m/2}$ . When  $G < G_c$  ( $G > G_c$ ),  $t_z$  is negative (positive). Under critical coupling, the amplitude at the cavity resonance becomes zero, indicating that the mechanically induced CPA (MCPA) occurs. The phase at zero detuning (cavity resonance) is given as  $\varphi_z = \arg(t_z)$ . It is notable that the imaginary part of  $t_z$  on resonance is always zero [i.e.,  $\text{Im}(t_z) = 0$ ]. We then have  $\tan(\varphi_z) = \text{Im}(t_z)/\text{Re}(t_z) = 0$ , and the nontrivial solutions for the phase at zero detuning are  $\varphi_z \in [0, \pi]$ . Because  $\cos(\varphi_z) \propto \text{Re}(t_z)$ , and the value of  $\cos(\varphi_z)$  is negative (positive) for  $G < G_c$  ( $G > G_c$ ), hence yielding a phase  $\varphi_z = \pi$  ( $\varphi_z = 0$ ), respectively. Remarkably, the MCPA mediates an abrupt  $\pi$ -phase transition at the critical coupling.

*Observation of the MCPA and anti-lasing.*—In earlier work, CPA and anti-lasing have been achieved by controlling the interference of multiple incident waves inside a thin film [33–35]. For cavity optomechanical systems, the probe light can be perfectly absorbed through the constructive interference with the down-converted pump tone from the blue-detuned sideband [61]. In this case, the interaction Hamiltonian is written as  $H_{\text{int}}/\hbar = G(a^\dagger b^\dagger + ab)$ , corresponding to parametric amplification [62–64]. Switching from blue-detuned to red-detuned driving can induce a change from constructive to destructive interference, giving rise to OMIT [65]. The interaction Hamiltonian becomes beam-splitter-like  $H_{\text{int}}/\hbar = G(a^\dagger b + b^\dagger a)$  as in the present case, with the transmission coefficient given in Eq. (3). If the cavity is undercoupled ( $\eta < 1/2$ ), e.g., for the devices studied in Refs. [50–52], destructive interference occurs, and only OMIT is observed (see detailed discussions in Sec. IV of Ref. [75]). However, as will be shown in this

work, with overcoupling ( $\eta > 1/2$ ), interference becomes constructive again and OMIA can occur.

For the experiment, the device is mounted on a cold plate with a cryogenic temperature of 10 mK inside a dilution refrigerator. The measurement setups are shown in Sec. III of Ref. [75]. For our device, the external coupling corresponds to overcoupling,  $\eta = 0.651$ , and the pump driving is red-detuned. The resonance frequencies of the cavity and of the mechanical resonator are measured to be  $\omega_c/2\pi = 5.318$  GHz and  $\omega_m/2\pi = 755.5$  kHz, respectively. The other parameters for this device are calibrated as  $\kappa/2\pi = 420$  kHz, and  $\gamma_m/2\pi = 9.7$  mHz. Detailed calibration processes can be found in Sec. V of Ref. [75]. Then, the calculated critical coupling is given as  $G_c/2\pi = 17.53$  Hz.

The amplitude response, with a coupling strength  $G/2\pi = 17.66$  Hz, is presented in Fig. 2(a). The amplitude at the absorption dip is nearly 50 dB lower than the baseline of the transmission spectrum. As shown in Fig. 2(b), the amplitude  $T_z$  at the cavity resonance is measured with a continuously increasing  $G$ . The amplitude  $T_z$  dramatically drops until  $G$  reaches  $G_c$ , and then starts to increase with further increasing the coupling strength. The MCPA occurs and anti-lasing is observed at  $G_c$ . Figure 2(b) shows that the measured critical coupling occurs at  $G_c/2\pi = 17.528$  Hz, which agrees well with the calculated value. The coupling strength corresponding to the boundary between absorption (anti-lasing) and transparency is given as  $G_b = \sqrt{(\eta/2 - 1/4)\kappa\gamma_m/(1 - \eta)}$ . For our device, the boundary coupling is  $G_b/2\pi = 29.68$  Hz. The inset in Fig. 2(a) [Fig. 2(b)] shows the typical amplitude response in the transparency (anti-lasing) regime, respectively.

The MCPA allows for the following physical interpretation. Optomechanical interaction of the pump and probe tones creates a sideband at the probe tone frequency. Below critical coupling ( $G < G_c$ ), the mechanical sideband is smaller than the probe tone, leading to only partial absorption, and the phase is that of the probe tone. At the critical coupling ( $G = G_c$ ), the sideband perfectly interferes with the probe field inside the cavity, leading

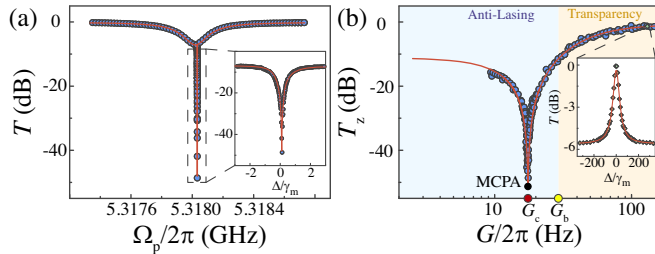


FIG. 2. (a) The transmission spectrum for the MCPA; and (b) the amplitude at cavity resonance versus coupling strength. Inset in (a) zooms inside the absorption dip. Inset in (b) demonstrates a typical transparent window in the transparency regime with  $G/2\pi = 176.8$  Hz. Blue circles: data; Red solid lines: fit. Blue (orange) background marks the anti-lasing (transparency) regime, respectively.

to coherent perfect absorption and no emitted field. Above critical coupling but below the boundary coupling ( $G_c < G < G_b$ ), the sideband now dominates over the probe, so that only part of the sideband tone is transmitted out of the cavity, being  $\pi$  out of phase with respect to the original probe tone. Above the boundary coupling ( $G > G_b$ ), the sideband is strong enough to increase the transmission beyond the bare microwave cavity background, and a transmission peak appears.

*The  $\pi$ -phase transition and phase slope flip.*—In the anti-lasing regime, for a specific value of  $T_z$ , there exist two coupling strengths which are located to the left or right of  $G_c$ , respectively. The phase responses for  $G/2\pi = 17.24$  and 17.84 Hz (corresponding to  $T_z = -42$  dB) are shown in Fig. 3(a). Under these two coupling strengths, although both the amplitude responses exhibit absorption dips [as shown in Fig. 2(a)], the phase at zero detuning undergoes an abrupt shift by  $\pi$  (referred to as  $\pi$ -phase transition). As the detuning becomes large, at the coupling values just above and below  $G_c$ , the phase becomes  $\pi$  at overcoupling, whereas undercoupling yields a zero phase [75]. Thus, switching from under- to overcoupling leads to the destructive interference (OMIT) changing into constructive interference (OMIA).

The phases  $\phi_z$  at the cavity resonance are measured for different coupling strengths  $G$  and are shown in Fig. 3(b). An obvious  $\pi$ -phase transition occurs at the critical coupling  $G_c$ , where all the inject microwave photons are absorbed ( $T_z$  becomes zero). Thus, the MCPA mediates such  $\pi$ -phase transition. The insets in Fig. 3(b) show a typical phase response, where  $G$  is located either on the left or right side of  $G_c$ . On the right side of  $G_c$ , it is notable that the phase response maintains the same line shape [as shown in the right inset in Fig. 3(b)] in both the anti-lasing and transparency regimes. It is also worthy to note that the  $\pi$ -phase transition further flips the slope in the frequency dependence of the phase, as shown in Fig. 3(a). For  $G < G_c$  ( $G > G_c$ ), the phase slope at zero detuning is always positive (negative), respectively, undergoing a positive-negative transition around the cavity resonance.

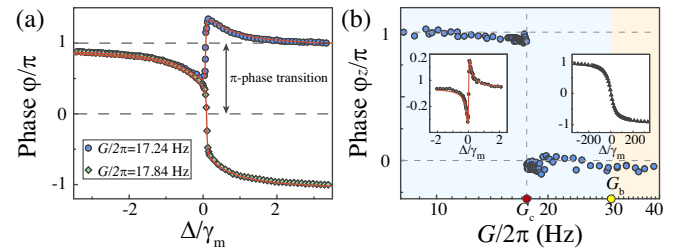


FIG. 3. (a) Phase  $\phi$  versus detuning  $\Delta$  for two coupling strengths close to the critical coupling  $G_c$  on both sides. (b) Phase  $\phi_z$  at cavity resonance versus coupling strength  $G$ . Insets in (b) illustrate typical phase response with coupling strengths on either side of  $G_c$ . Red and black solid lines: fit; Circles, rhombuses, and triangles: data.

Thus, the phase slope at  $G_c$  is discontinuous, which indicates a singularity for the phase slope.

*Infinite discontinuity and a singularity in the group delay.*—Group delay is given by  $\tau = \partial\phi/\partial\Omega_p = -\partial\phi/\partial\Delta$ . Hence, multiplying the phase slope by a negative sign implies a group delay. Thus, a singularity exists in the group velocity in our case. In the experiment, the group delay is initially measured at several frequencies of the probe tone, which is generated and further analyzed by a vector network analyzer (VNA).

Figures 4(a)–4(c) show the measured group delay  $\tau$  for three different coupling strengths. The corresponding phase responses have been presented in Fig. 3(a), and the right inset in Fig. 3(b), respectively. Figure 4(a) shows group advance with a coupling  $G/2\pi = 17.24$  Hz, and Fig. 4(b) shows group delay with a coupling  $G/2\pi = 17.84$  Hz. These two coupling strengths are inside the anti-lasing regime and very close to  $G_c$  from either side. However, the amplitude responses around  $G_c$  only exhibit absorption dips, as shown in Fig. 2(a). Figure 4(c) shows group delay with a coupling  $G > G_b$  in the transparency regime, and its corresponding amplitude response has been shown in the inset of Fig. 2(b).

The group delay at the cavity resonance  $\tau_z$  versus different coupling strengths is demonstrated in Fig. 4(d). Fast (slow) light with negative (positive) group delay are observed on the left (right) sides of  $G_c$ , respectively. The group advance and delay approach infinity at  $G_c$ . Thus, the  $\pi$ -phase transition and the phase slope flip result in a

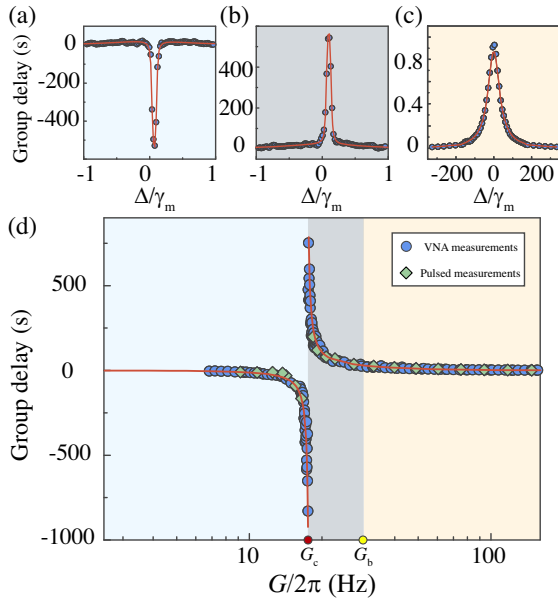


FIG. 4. Group delay  $\tau$  versus detuning  $\Delta$  are shown in (a) with  $G/2\pi = 17.24$  Hz, (b) with  $G/2\pi = 17.84$  Hz, and (c) with  $G/2\pi = 176.8$  Hz, respectively. (d) The group delay at zero detuning ( $\tau_z$ ) versus coupling strength  $G$  are measured. Blue circles (green rhombuses) mark the VNA (pulsed) measurements. Red solid lines: fit.

singularity in group delay with an infinite discontinuity, located at  $G_c$ . Compared to group delay in the transparency (or OMIT) regime extensively discussed in the literature [50–60], the group delay around the singularity is greatly enhanced or even diverges.

*Pulsed measurements.*—To directly explore the group delay, microwave pulses are generated by modulating the amplitude of a probe tone derived from a microwave generator. The Gaussian-shaped envelopes are generated with an arbitrary waveform generator. To avoid any pulse distortion in group delay measurements, the pulse bandwidths are chosen to be narrower than the transparency (absorption) window width. The emission of a probe pulse is synchronized with the acquisition of the transmitted probe field [75]. The group delay is given by the difference between the measured pulse center time (time at peak center) with and without a continuous-wave pump tone sent into the cavity.

In the anti-lasing regime, a group advance [as shown in Figs. 5(a) and 5(b)] is achieved, when  $G$  is located on the left side of the singularity (e.g.,  $G/2\pi = 11.87$  Hz). Figures 5(c) and 5(d) show a typical group delay when  $G$  is to the right from the singularity (e.g.,  $G/2\pi = 23.93$  Hz). In the transparency regime, a regular group delay is measured [as shown in Figs. 5(c) and 5(d)] with, e.g.,  $G/2\pi = 155.1$  Hz. The maximum group delay ( $\tau_m$ ) occurs at the zero detuning point.

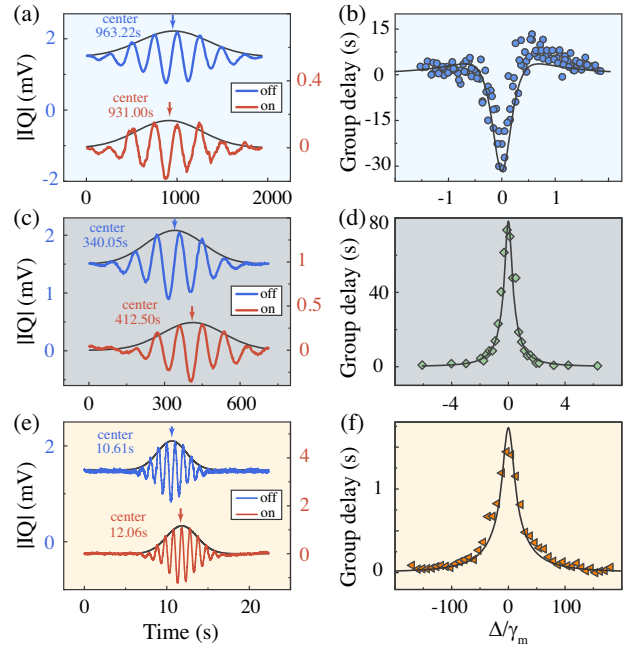


FIG. 5. Pulses propagating at cavity resonance are shown in (a), (c), and (e) with different coupling strengths. The extracted group delay versus  $\Delta$  are given in (b), (d), and (f), respectively. The coupling strength is fixed at  $G/2\pi = 11.87$  Hz for (a) and (b);  $G/2\pi = 23.93$  Hz for (c) and (d);  $G/2\pi = 155.1$  Hz for (e) and (f). Red solid lines (blue solid lines): Gaussian-shaped pulse is measured with (without) the pump tone. Black solid lines: fit.



It is notable that the maximum group delay is proportional to the mechanical lifetime (i.e.,  $\tau_m \propto 1/\gamma_m$ ) in the transparency regime [51,59,60]. Assisted by a low mechanical damping ( $\gamma_m = 9.7$  mHz), the measured maximum group delay in Fig. 5(f) arrives at  $\tau_m = 1.2$  s, which is an improvement of 8 orders of magnitude compared to 50 ns measured in optomechanical crystals, e.g., in Ref. [51] and 3 orders of magnitude improvement over 3 ms measured earlier in circuit electromechanics [59]. The measured group advance and delay, when probe-tone detuning is varied, exhibit an excellent agreement with our model. The measured group delay in a pulsed measurement also agrees well with the VNA group delay measurements (see Sec. VI of Ref. [75]).

**Conclusion.**—We experimentally study anti-lasing and MCPA, and find the latter occurs at a critical optomechanical coupling. Meanwhile, MCPA (anti-lasing) mediates a  $\pi$ -phase transition, which further flips the phase slope at cavity resonance. Subsequently, the group delay measured with a continuous or pulsed probe field exhibits a singularity, around which the group advance and delay diverge. An abrupt transition from an infinite group advance to delay is observed at this singularity. The  $\pi$ -phase transition and group-delay singularity could be further explored within an amplification regime by, e.g., utilizing blue-detuned sideband driving, to overcome the absorption loss [75]. The singularity with the infinite group delay may motivate ways to realize extremely long signal storage times as an alternative to the schemes based on, e.g., solid nuclear spins [82], or an atomic frequency comb [83]. Our scheme could also be realized in several other cavity-based quantum systems such as the cavity spintronics [84], circuit QED [85], and microcavity photonics [86].

This work is supported by the National Key Research and Development Program of China (Grant No. 2016YFA0301200), the National Natural Science Foundation of China (Grant No. 12004044, Grants No. 62074091 and No. U1930402), and Science Challenge Project (Grant No. TZ2018003), and by the Academy of Finland (Contracts No. 307757, No. 312057, No. 336810).

\*mika.sillanpaa@aalto.fi

†litf@tsinghua.edu.cn

- [1] M. Fleischhauer, A. Imamoglu, and J. P. Marangos, Electromagnetically induced transparency: Optics in coherent media, *Rev. Mod. Phys.* **77**, 633 (2005).
- [2] Y.-C. Liu, B.-B. Li, and Y.-F. Xiao, Electromagnetically induced transparency in optical microcavities, *Nanophotonics* **6**, 789 (2017).
- [3] X. Gu, A. F. Kockum, A. Miranowicz, Y.-X. Liu, and F. Nori, Microwave photonics with superconducting quantum circuits, *Phys. Rep.* **718–719**, 1 (2017).
- [4] A. M. Akulshin, S. Barreiro, and A. Lezama, Electromagnetically induced absorption and transparency due to resonant two-field excitation of quasidegenerate levels in Rb vapor, *Phys. Rev. A* **57**, 2996 (1998).
- [5] A. Lezama, S. Barreiro, and A. M. Akulshin, Electromagnetically induced absorption, *Phys. Rev. A* **59**, 4732 (1999).
- [6] A. V. Taichenachev, A. M. Tumaikin, and V. I. Yudin, Electromagnetically induced absorption in a four-state system, *Phys. Rev. A* **61**, 011802(R) (1999).
- [7] A. Lipsich, S. Barreiro, A. M. Akulshin, and A. Lezama, Absorption spectra of driven degenerate two-level atomic systems, *Phys. Rev. A* **61**, 053803 (2000).
- [8] C. Goren, A. D. Wilson-Gordon, M. Rosenbluh, and H. Friedmann, Electromagnetically induced absorption due to transfer of coherence and to transfer of population, *Phys. Rev. A* **67**, 033807 (2003).
- [9] J. Sheng, X. Yang, U. Khadka, and M. Xiao, All-optical switching in an n-type four-level atom-cavity system, *Opt. Express* **19**, 17059 (2011).
- [10] G. Romero, J. J. García-Ripoll, and E. Solano, Microwave Photon Detector in Circuit QED, *Phys. Rev. Lett.* **102**, 173602 (2009).
- [11] B. Peropadre, G. Romero, G. Johansson, C. M. Wilson, E. Solano, and J. J. García-Ripoll, Approaching perfect microwave photodetection in circuit QED, *Phys. Rev. A* **84**, 063834 (2011).
- [12] M. K. Akhlaghi, E. Schelew, and J. F. Young, Waveguide integrated superconducting single-photon detectors implemented as near-perfect absorbers of coherent radiation, *Nat. Commun.* **6**, 8233 (2015).
- [13] D. Floess, M. Hentschel, T. Weiss, H.-U. Habermeier, J. Jiao, S. G. Tikhodeev, and H. Giessen, Plasmonic Analog of Electromagnetically Induced Absorption Leads to Giant Thin Film Faraday Rotation of 14°, *Phys. Rev. X* **7**, 021048 (2017).
- [14] N. Thaicharoen, K. R. Moore, D. A. Anderson, R. C. Powell, E. Peterson, and G. Raithel, Electromagnetically induced transparency, absorption, and microwave-field sensing in a Rb vapor cell with a three-color all-infrared laser system, *Phys. Rev. A* **100**, 063427 (2019).
- [15] K.-Y. Liao, H.-T. Tu, S.-Z. Yang, C.-J. Chen, X.-H. Liu, J. Liang, X.-D. Zhang, H. Yan, and S.-L. Zhu, Microwave electrometry via electromagnetically induced absorption in cold rydberg atoms, *Phys. Rev. A* **101**, 053432 (2020).
- [16] Zeeshan Ali Safdar Jadoon, H.-R. Noh, and J.-T. Kim, Multiphoton nonlinear frequency mixing effects on the coherent electromagnetically induced absorption spectra of  $^{85}\text{Rb}$  atoms under a longitudinal magnetic field: Theory and experiment, *Phys. Rev. A* **102**, 063714 (2020).
- [17] J. Dimitrijević, D. Arsenović, and B. M. Jelenković, Coherent processes in electromagnetically induced absorption: A steady and transient study, *New J. Phys.* **13**, 033010 (2011).
- [18] X. Zhang, N. Xu, K. Qu, Z. Tian, R. Singh, J. Han, G. S. Agarwal, and W. Zhang, Electromagnetically induced absorption in a three-resonator metasurface system, *Sci. Rep.* **5**, 10737 (2015).
- [19] M. F. Limonov, M. V. Rybin, A. N. Poddubny, and Y. S. Kivshar, Fano resonances in photonics, *Nat. Photonics* **11**, 543 (2017).

- [20] A. S. Shakthi, A. B. Yelikar, and R. Pant, Analogue of electromagnetically induced absorption in the microwave domain using stimulated brillouin scattering, *Commun. Phys.* **3**, 109 (2020).
- [21] G. S. Agarwal and Y. Zhu, Photon trapping in cavity quantum electrodynamics, *Phys. Rev. A* **92**, 023824 (2015).
- [22] G. S. Agarwal, K. Di, L. Wang, and Y. Zhu, Perfect photon absorption in the nonlinear regime of cavity quantum electrodynamics, *Phys. Rev. A* **93**, 063805 (2016).
- [23] L. Wang, K. Di, Y. Zhu, and G. S. Agarwal, Interference control of perfect photon absorption in cavity quantum electrodynamics, *Phys. Rev. A* **95**, 013841 (2017).
- [24] Y.-h. Wei, W.-j. Gu, G. Yang, Y. Zhu, and G.-x. Li, Coherent perfect absorption in a quantum nonlinear regime of cavity quantum electrodynamics, *Phys. Rev. A* **97**, 053825 (2018).
- [25] W. Xiong, J. Chen, B. Fang, C.-H. Lam, and J. Q. You, Coherent perfect absorption in a weakly coupled atom-cavity system, *Phys. Rev. A* **101**, 063822 (2020).
- [26] D. G. Baranov, A. Krasnok, T. Shegai, A. Alù, and Y. Chong, Coherent perfect absorbers: Linear control of light with light, *Nat. Rev. Mater.* **2**, 17064 (2017).
- [27] D. Zhang, X.-Q. Luo, Y.-P. Wang, T.-F. Li, and J. Q. You, Observation of the exceptional point in cavity magnon-polaritons, *Nat. Commun.* **8**, 1368 (2017).
- [28] J.-H. Wu, M. Artoni, and G. C. La Rocca, Coherent perfect absorption in one-sided reflectionless media, *Sci. Rep.* **6**, 35356 (2016).
- [29] J.-H. Wu, M. Artoni, and G. C. La Rocca, Perfect absorption and no reflection in disordered photonic crystals, *Phys. Rev. A* **95**, 053862 (2017).
- [30] T. Roger, S. Vezzoli, E. Bolduc, J. Valente, J. J. F. Heitz, J. Jeffers, C. Soci, J. Leach, C. Couteau, N. I. Zheludev, and D. Faccio, Coherent perfect absorption in deeply subwavelength films in the single-photon regime, *Nat. Commun.* **6**, 7031 (2015).
- [31] Y. Li and C. Argyropoulos, Tunable nonlinear coherent perfect absorption with epsilon-near-zero plasmonic waveguides, *Opt. Lett.* **43**, 1806 (2018).
- [32] A. Berkhout and A. F. Koenderink, Perfect absorption and phase singularities in plasmon antenna array etalons, *ACS Photonics* **6**, 2917 (2019).
- [33] Y. D. Chong, L. Ge, H. Cao, and A. D. Stone, Coherent Perfect Absorbers: Time-Reversed Lasers, *Phys. Rev. Lett.* **105**, 053901 (2010).
- [34] W. Wan, Y. Chong, L. Ge, H. Noh, A. D. Stone, and H. Cao, Time-reversed lasing and interferometric control of absorption, *Science* **331**, 889 (2011).
- [35] A. D. Stone, Gobbling up light with an antilaser, *Phys. Today* **64**, No. 11, 68 (2011).
- [36] Z. J. Wong, Y.-L. Xu, J. Kim, K. O'Brien, Y. Wang, L. Feng, and X. Zhang, Lasing and anti-lasing in a single cavity, *Nat. Photonics* **10**, 796 (2016).
- [37] K. Pichler, M. Kühmayer, J. Böhm, A. Brandstötter, P. Ambichl, U. Kuhl, and S. Rotter, Random anti-lasing through coherent perfect absorption in a disordered medium, *Nature (London)* **567**, 351 (2019).
- [38] R. W. Boyd, Slow and fast light: Fundamentals and applications, *J. Mod. Opt.* **56**, 1908 (2009).
- [39] H. Ian, Y.-x. Liu, and F. Nori, Tunable electromagnetically induced transparency and absorption with dressed superconducting qubits, *Phys. Rev. A* **81**, 063823 (2010).
- [40] B.-B. Li, Y.-F. Xiao, C.-L. Zou, Y.-C. Liu, X.-F. Jiang, Y.-L. Chen, Y. Li, and Q. Gong, Experimental observation of fano resonance in a single whispering-gallery microresonator, *Appl. Phys. Lett.* **98**, 021116 (2011).
- [41] B. Peng, Ş. K. Özdemir, W. Chen, F. Nori, and L. Yang, What is and what is not electromagnetically induced transparency in whispering-gallery microcavities, *Nat. Commun.* **5**, 5082 (2014).
- [42] H. Lü, C. Wang, L. Yang, and H. Jing, Optomechanically Induced Transparency at Exceptional Points, *Phys. Rev. Applied* **10**, 014006 (2018).
- [43] J. Zhao, L. Wu, T. Li, Y.-x. Liu, F. Nori, Y. Liu, and J. Du, Phase-Controlled Pathway Interferences and Switchable Fast-Slow Light in a Cavity-Magnon Polariton System, *Phys. Rev. Applied* **15**, 024056 (2021).
- [44] R. Taubert, M. Hentschel, J. Kästel, and H. Giessen, Classical analog of electromagnetically induced absorption in plasmonics, *Nano Lett.* **12**, 1367 (2012).
- [45] P. Tassin, L. Zhang, R. Zhao, A. Jain, T. Koschny, and C. M. Soukoulis, Electromagnetically Induced Transparency and Absorption in Metamaterials: The Radiating Two-Oscillator Model and its Experimental Confirmation, *Phys. Rev. Lett.* **109**, 187401 (2012).
- [46] C. Yang, X. Jiang, Q. Hua, S. Hua, Y. Chen, J. Ma, and M. Xiao, Realization of controllable photonic molecule based on three ultrahigh-Q microtoroid cavities, *Laser Photonics Rev.* **11**, 1600178 (2017).
- [47] G. S. Agarwal and S. Huang, Electromagnetically induced transparency in mechanical effects of light, *Phys. Rev. A* **81**, 041803(R) (2010).
- [48] S. Huang and G. S. Agarwal, Electromagnetically induced transparency with quantized fields in optocavity mechanics, *Phys. Rev. A* **83**, 043826 (2011).
- [49] K. Qu and G. S. Agarwal, Phonon-mediated electromagnetically induced absorption in hybrid opto-electromechanical systems, *Phys. Rev. A* **87**, 031802(R) (2013).
- [50] S. Weis, R. Rivière, S. Deléglise, E. Gavartin, O. Arcizet, A. Schliesser, and T. J. Kippenberg, Optomechanically induced transparency, *Science* **330**, 1520 (2010).
- [51] A. H. Safavi-Naeini, T. M. Alegre, J. Chan, M. Eichenfield, M. Winger, Q. Lin, J. T. Hill, D. E. Chang, and O. Painter, Electromagnetically induced transparency and slow light with optomechanics, *Nature (London)* **472**, 69 (2011).
- [52] M. Karuza, C. Biancofiore, M. Bawaj, C. Molinelli, M. Galassi, R. Natali, P. Tombesi, G. Di Giuseppe, and D. Vitali, Optomechanically induced transparency in a membrane-in-the-middle setup at room temperature, *Phys. Rev. A* **88**, 013804 (2013).
- [53] C. Dong, V. Fiore, M. C. Kuzyk, and H. Wang, Transient optomechanically induced transparency in a silica microsphere, *Phys. Rev. A* **87**, 055802 (2013).
- [54] C.-H. Dong, Z. Shen, C.-L. Zou, Y.-L. Zhang, W. Fu, and G.-C. Guo, Brillouin-scattering-induced transparency and non-reciprocal light storage, *Nat. Commun.* **6**, 6193 (2015).
- [55] J. Kim, M. C. Kuzyk, K. Han, H. Wang, and G. Bahl, Non-reciprocal brillouin scattering induced transparency, *Nat. Phys.* **11**, 275 (2015).

- [56] J. D. Teufel, D. Li, M. S. Allman, K. Cicak, A. J. Sirois, J. D. Whittaker, and R. W. Simmonds, Circuit cavity electromechanics in the strong-coupling regime, *Nature (London)* **471**, 204 (2011).
- [57] C. F. Ockeloen-Korppi, M. F. Gely, E. Damskäg, M. Jenkins, G. A. Steele, and M. A. Sillanpää, Sideband cooling of nearly degenerate micromechanical oscillators in a multimode optomechanical system, *Phys. Rev. A* **99**, 023826 (2019).
- [58] F. Massel, S. U. Cho, J.-M. Pirkkalainen, P. J. Hakonen, T. T. Heikkilä, and M. A. Sillanpää, Multimode circuit optomechanics near the quantum limit, *Nat. Commun.* **3**, 987 (2012).
- [59] X. Zhou, F. Hocke, A. Schliesser, A. Marx, H. Huebl, R. Gross, and T. J. Kippenberg, Slowing, advancing and switching of microwave signals using circuit nanoelectromechanics, *Nat. Phys.* **9**, 179 (2013).
- [60] L. Fan, K. Y. Fong, M. Poot, and H. X. Tang, Cascaded optical transparency in multimode-cavity optomechanical systems, *Nat. Commun.* **6**, 5850 (2015).
- [61] F. Hocke, X. Zhou, A. Schliesser, T. J. Kippenberg, H. Huebl, and R. Gross, Electromechanically induced absorption in a circuit nano-electromechanical system, *New J. Phys.* **14**, 123037 (2012).
- [62] F. Massel, T. Heikkilä, J.-M. Pirkkalainen, S.-U. Cho, H. Saloniemi, P. J. Hakonen, and M. A. Sillanpää, Microwave amplification with nanomechanical resonators, *Nature (London)* **480**, 351 (2011).
- [63] K. Y. Fong, L. Fan, L. Jiang, X. Han, and H. X. Tang, Microwave-assisted coherent and nonlinear control in cavity piezo-optomechanical systems, *Phys. Rev. A* **90**, 051801(R) (2014).
- [64] X. Zhang, C.-L. Zou, L. Jiang, and H. X. Tang, Cavity magnomechanics, *Sci. Adv.* **2**, e1501286 (2016).
- [65] M. Aspelmeyer, T. J. Kippenberg, and F. Marquardt, Cavity optomechanics, *Rev. Mod. Phys.* **86**, 1391 (2014).
- [66] H. Xiong and Y. Wu, Fundamentals and applications of optomechanically induced transparency, *Appl. Phys. Rev.* **5**, 031305 (2018).
- [67] Y.-L. Liu, C. Wang, J. Zhang, and Y.-x. Liu, Cavity optomechanics: Manipulating photons and phonons towards the single-photon strong coupling, *Chin. Phys. B* **27**, 024204 (2018).
- [68] I. C. Rodrigues, D. Bothner, and G. A. Steele, Coupling microwave photons to a mechanical resonator using quantum interference, *Nat. Commun.* **10**, 5359 (2019).
- [69] J.-M. Pirkkalainen, S. U. Cho, J. Li, G. S. Paraoanu, P. J. Hakonen, and M. A. Sillanpää, Hybrid circuit cavity quantum electrodynamics with a micromechanical resonator, *Nature (London)* **494**, 211 (2013).
- [70] T. Bera, S. Majumder, S. K. Sahu, and V. Singh, Large flux-mediated coupling in hybrid electromechanical system with a transmon qubit, *Commun. Phys.* **4**, 12 (2021).
- [71] F. Lecocq, J. D. Teufel, J. Aumentado, and R. W. Simmonds, Resolving the vacuum fluctuations of an optomechanical system using an artificial atom, *Nat. Phys.* **11**, 635 (2015).
- [72] D. Zopf, M. L. Juan, C. M. F. Schneider, and G. Kirchmair, Single-Photon Cooling in Microwave Magnetomechanics, *Phys. Rev. Lett.* **125**, 023601 (2020).
- [73] M. Mirhosseini, A. Sipahigil, M. Kalaei, and O. Painter, Superconducting qubit to optical photon transduction, *Nature (London)* **588**, 599 (2020).
- [74] B. Chen, H.-W. Xing, J.-B. Chen, H.-B. Xue, and L.-L. Xing, Tunable fast-slow light conversion based on optomechanically induced absorption in a hybrid atom-optomechanical system, *Quantum Inf. Process.* **20**, 10 (2021).
- [75] See Supplemental Material at <http://link.aps.org/supplemental/10.1103/PhysRevLett.127.273603> for (i) the device, (ii) electromagnetic distribution, (iii) measurement setups, (iv) simulations of  $\pi$ -phase transition, (v) device parameter calibration, and (vi) the vna group delay measurements,.
- [76] M. Yuan, V. Singh, Y. M. Blanter, and G. A. Steele, Large cooperativity and microkelvin cooling with a three-dimensional optomechanical cavity, *Nat. Commun.* **6**, 8491 (2015).
- [77] M. Yuan, M. A. Cohen, and G. A. Steele, Silicon nitride membrane resonators at millikelvin temperatures with quality factors exceeding  $10^8$ , *Appl. Phys. Lett.* **107**, 263501 (2015).
- [78] A. Noguchi, R. Yamazaki, M. Ataka, H. Fujita, Y. Tabuchi, T. Ishikawa, K. Usami, and Y. Nakamura, Ground state cooling of a quantum electromechanical system with a silicon nitride membrane in a 3D loop-gap cavity, *New J. Phys.* **18**, 103036 (2016).
- [79] A. H. Ghadimi, S. A. Fedorov, N. J. Engelsen, M. J. Breyhi, R. Schilling, D. J. Wilson, and T. J. Kippenberg, Elastic strain engineering for ultralow mechanical dissipation, *Science* **360**, 764 (2018).
- [80] Y. Tsaturyan, A. Barg, E. S. Polzik, and A. Schliesser, Ultracoherent nanomechanical resonators via soft clamping and dissipation dilution, *Nat. Nanotechnol.* **12**, 776 (2017).
- [81] G. S. MacCabe, H. Ren, J. Luo, J. D. Cohen, H. Zhou, A. Sipahigil, M. Mirhosseini, and O. Painter, Nano-acoustic resonator with ultralong phonon lifetime, *Science* **370**, 840 (2020).
- [82] M. Zhong, M. P. Hedges, R. L. Ahlefeldt, J. G. Bartholomew, S. E. Beavan, S. M. Wittig, J. J. Longdell, and M. J. Sellars, Optically addressable nuclear spins in a solid with a six-hour coherence time, *Nature (London)* **517**, 177 (2015).
- [83] Y. Ma, Y.-Z. Ma, Z.-Q. Zhou, C.-F. Li, and G.-C. Guo, One-hour coherent optical storage in an atomic frequency comb memory, *Nat. Commun.* **12**, 2381 (2021).
- [84] Y.-P. Wang and C.-M. Hu, Dissipative couplings in cavity magnonics, *J. Appl. Phys.* **127**, 130901 (2020).
- [85] S. Haroche, M. Brune, and J. M. Raimond, From cavity to circuit quantum electrodynamics, *Nat. Phys.* **16**, 243 (2020).
- [86] W. Chen, D. Leykam, Y. Chong, and L. Yang, Nonreciprocity in synthetic photonic materials with nonlinearity, *MRS Bull.* **43**, 443 (2018).